Identification of source velocities on 3D structures in non-anechoic environments: Theoretical background and experimental validation of the inverse patch transfer functions method

M. Aucejo, N. Totaro, J.-L. Guyader

Identification of source velocities on 3D structures in non-anechoic environments: Theoretical background and Experimental Validation of the inverse Patch Transfer Functions Method

M. Aucejo[1], N. Totaro, J-L. Guyader

Laboratoire Vibrations Acoustique, INSA Lyon, 25 bis avenue Jean Capelle 69621 Villeurbanne Cedex, FRANCE

Abstract

In noise control, the identification of source velocity field remains an important and open problem. In this way, methods such as Nearfield Acoustical Holography (NAH), Principal Source Projection (PSP), inverse Frequency Response Function method (iFRF) or hybrid NAH have been developed. However, these methods require free field conditions that are often difficult to achieve in practice. In this article, an alternative method, developed in the SILENCE European project framework and called inverse Patch Transfer Functions, is presented to identify source velocities. This method is based on the definition of a virtual cavity, the double measurement of the pressure and particle velocity fields on aperture surfaces of this volume, divided into elementary areas called patches and the inversion of impedances matrices, numerically computed from a modal basis obtained by FEM. Theoretically, the method is applicable to sources with complex 3D geometries and measurements can be carried out in a non-anechoic environment even in the presence of other stationary sources outside the virtual cavity. In the present paper, theoretical background of the iPTF method is exposed and results (numerical and experimental) on a source with simple geometry (two baffled pistons driven in antiphase) are presented and discussed.

Key words: Holography, FEM, Patch,Transfer Functions

*Corresponding author. Fax : 33.4.72.43.87.12. E-mail address : mathieu.aucejo@insa-lyon.fr

1. Introdution

The Nearfield Acoustical Holography (NAH), firstly introduced by Williams et al. [1, 2], is based on the two-dimensional Fourier Transform of the complex pressure field at a given frequency measured on a hologram near the source. Measurements of the pressure field are generally made on a plane surface and make possible the determination of the three-dimensional source velocity field. However, the NAH is mainly applicable to simple geometries (planes [3], cylinders [4] and spheres [5]). Furthermore, problems of discontinuities exist at boundaries, because of the lack of information beyond the zone of measurements nevertheless necessary to compute the two-dimensional Fourier Transform. Thus, to avoid the influence of boundary effects, measurements have to be made in the acoustical nearfield of the structure.

The iFRF method is based on the evaluation and the inversion of transfer matrices, which can be obtained either experimentally or numerically. In the last case, if the computation of the transfer functions is based on the Boundary Element Method, it is called iBEM. This method can be used to reconstruct acoustic radiation on arbitrary surfaces [6]. In that way, Martinus [7] uses this method to determine the distribution of particle velocity on the open end of a rectangular duct and shows that sound pressure field measurements need not to be made in the nearfield of the source to obtain good results. However, the main drawback of iBEM is that it requires an excessive amount of measurements to determine the acoustic field on a complex structure, since it needs a fine mesh definition (six nodes per wavelength). The difficulty of the method comes also from the inversion of the transfer matrices, which are often ill-conditioned and thus requires the use of regularization methods.

Other methods are also developed to overcome the difficulties and limitations inherent to NAH or iBEM. Thus, a hybrid NAH was introduced [8, 9]. This method is based on a modified HELS method (Helmholtz Equation Least Squares) [10, 11] and allows a reconstruction of the pressure field on a complex shape surface very close to the source surface. As NAH applications, the hybrid NAH needs regularization, because of measuring uncertainty and incompleteness of acoustic pressure field, which leads to ill-conditioned trans-

fer matrices. Furthermore, the modified HELS method can be also combined with iBEM [12] to reconstruct acoustic quantities on a virtual sphere enclosing the source structure, which can lead to the loss of nearfield information. Finally to avoid a great number of measurements, the PSP (Principal Source Projection) method is introduced [13, 14]. This method is based on the evaluation of a radiation operator between the source surface, represented by a distribution of elementary sources, and a grid of measurements. For traditional methods, like iBEM, the number of identified acoustic sources is limited to the number of microphones in order to guarantee the uniqueness of the solution. On the contrary, for PSP method, the number of quantified sources is higher than the number of microphones, which means that the system is under-determined. In addition, to identify the data on the source surface, the transfer functions, calculated between a point of the elementary source and a point of measurement, have to be inverted. The transfer matrix is often ill-conditioned, which implies to use regularization methods like Truncated Singular Values Decomposition (TSVD).

In this article, an alternative method is introduced to identify source velocities: the iPTF method. This method is derived from the Patch Transfer Functions (PTF) method [15, 16, 17]. In its direct formulation, the PTF method is a tool to predict pressure inside and outside a cavity containing acoustic sources and apertures, thanks to the use of substructuring and impedance concepts. The acoustical medium is indeed divided into subdomains and PTF are evaluated by suitable methods for each subdomain (FEM, Rayleigh approach, measurements, ...). Subdomains are then coupled through their common surface, divided into patches. Coupling conditions are written for each patch as pressure and velocity equations, describing the local equilibrium. A system of linear equations is finally obtained, where unknowns are coupling patch velocities. The system is solved to determine coupling velocities and finally pressures at any point of the acoustical domain.

The aim of the inverse approach (iPTF method) is to determine source velocities from measured patch pressures and velocities on a virtual cavity. Theoretically, iPTF method allows identifying source velocities in a noisy environment (i.e. in the presence of other sources) thanks to double measurements of pressure and particle velocity fields on a surface surrounding the source, what is not possible with classical methods, which only use sound pressure measurements. Measurements can thus be made, for instance, on a

part of an engine in use. However, as classically observed in inverse methods, the inversion of an ill-conditioned matrix is required. But this drawback can be alleviate by using suitable regularization techniques like TSVD or Tikhonov. Finally, one of the advantages of iPTF method is the use of the Finite Element Method (FEM) as a solver. When other methods need analytical or BEM model to estimate transfer functions, iPTF only needs modal basis of a virtual cavity to compute Patch Transfer Functions. This makes the method applicable even to sources with complex geometries.

The present article deals with the theoretical background of the method and its numerical and experimental application on a simple case (two baffled pistons driven in antiphase). This test case is voluntarily simple in order to easily study the main features of the proposed method, namely the size of the virtual cavity, the number of measurement patches, the ability to localize and separate sources and finally the robustness of the method with respect to an external stationnary disturbing source. Experimental validations of the iPTF approach confirm expected advantages and demonstrate the applicability of the method.

2. Theoretical background of the iPTF method

2.1. Basic concept of the iPTF method: the integral formulation

Let us consider the acoustic cavity presented in Fig. (1). The acoustical domain Ω is delimited by a rigid surface S_r, an absorbing surface S_a, a vibrating surface S_v and a surface with Dirichlet conditions S_d. Furthermore, an acoustic source S_0 is located inside the acoustic volume Ω, but outside a part Ω_c of Ω. Consequently, the problem to solve is expressed by Eq. (1)

$$\begin{cases} \Delta p(M) + k^2 p(M) = S_0(M) & \forall M \in \Omega \\ \dfrac{\partial p}{\partial n}(Q) = 0 & \forall Q \in S_r \\ \dfrac{\partial p}{\partial n}(Q) = -j\rho\omega V(Q) & \forall Q \in S_v \\ p(Q) = p_0 & \forall Q \in S_d \\ p(Q) = -\dfrac{Z}{j\rho\omega}\dfrac{\partial p}{\partial n}(Q) & \forall Q \in S_a \end{cases} \tag{1}$$

Where Δ is the Laplacian operator, $\frac{\partial}{\partial n}$ the normal derivative, ρ the density of air, $V(Q)$ the normal velocity imposed on S_v, p_0 the pressure imposed

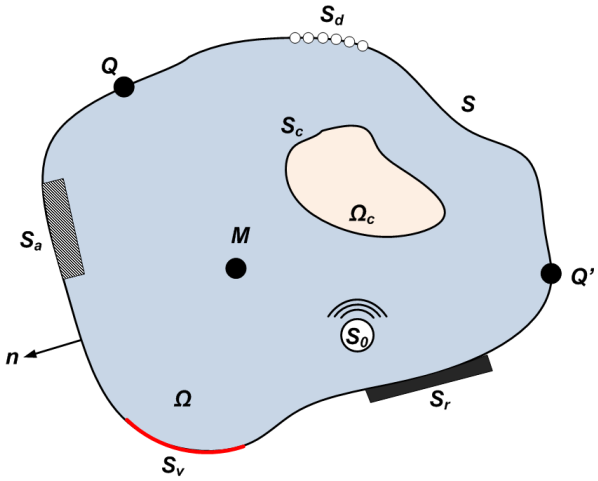

Figure 1: Integral problem

on S_d, Z the surface impedance of the absorbing material, ω the radian frequency and k the acoustic wavenumber.

Now, let us write the Green's identity given by Eq. (2) applied to the volume $\Omega_c \subset \Omega$.

$$\iiint_{\Omega_c} \left(\left[\Delta\Phi + k^2\Phi\right] \Psi - \left[\Delta\Psi + k^2\Psi\right] \Phi \right) d\Omega_c = \iint_{S_c} \left(\Phi \frac{\partial \Psi}{\partial n} - \Psi \frac{\partial \Phi}{\partial n} \right) dS_c \tag{2}$$

The previous expression is very general and functions Φ and Ψ are arbitrary. In the present work, we suppose first that the function Φ is the acoustic pressure p. In the cavity Ω_c, where no sources acting, the pressure satisfies the homogeneous Helmholtz equation as expressed in Eq. (3),

$$\Delta p(M) + k^2 p(M) = 0 \quad \forall M \in \Omega_c \tag{3}$$

The function Ψ is chosen as the Green's function G satisfaying Eq. (4).

$$\begin{cases} \Delta G(M, M') + k^2 G(M, M') = 0 & \forall (M, M') \in \Omega_c \\ \dfrac{\partial G}{\partial n}(Q, Q') = \delta(Q - Q') & \forall (Q, Q') \in S_c \end{cases} \tag{4}$$

Consequently, by introducing Eqs. (3) and (4) in Eq. (2), we finally obtain the integral equation given by Eq. (5).

$$p(Q') = \iint_{S_c} G(Q,Q') \frac{\partial p}{\partial n}(Q) dQ \tag{5}$$

The key point of this formulation is that external sources located outside the cavity do not modify the integral equation. In other words, this formulation is independent of acoustic sources external to Ω_c. Furthermore, another asset of integral formulation method is that the Green's function G can be arbitrarily chosen. To illustrate this point, let us consider the Green's function G' satisfaying Dirichlet's boundary condition as expressed in Eq. (6)).

$$\begin{cases} \Delta G'(M,M') + k^2 G'(M,M') = 0 & \forall (M,M') \in \Omega_c \\ G'(Q,Q') = \delta(Q-Q') & \forall (Q,Q') \in S_c \end{cases} \tag{6}$$

The introduction of Eqs. (3) and (6) in Eq. (2) allows obtaining the integral formulation given by Eq. (7), which is independent of external acoustic sources too.

$$\frac{\partial p}{\partial n}(Q') = \iint_{S_c} p(Q) \frac{\partial G'}{\partial n}(Q,Q') dQ \tag{7}$$

2.2. Basic equation of the iPTF method

Let us consider the practical situation given in Fig. (2), where a virtual cavity of surface $S_c = S_m \cup S_v$ surrounds the source and separates the acoustical domain into a virtual cavity Ω_c and an exterior domain Ω_e.

In the iPTF formulation, the Green's function used is that of virtual cavity where boundary surface S_c is supposed rigid. It is important to notice that these rigid wall boundary conditions have no physical reality. They just provide a mathematical tool to solve the virtual cavity problem. The integral formulation to solve is consequently the one given by Eq. (5). When using Euler's equation in Eq. (5), the acoustic pressure $p(Q')$ at the point Q' is related to the normal velocity $V_n(Q)$ at each point Q of the surface S_c as expressed in Eq. (8).

$$p(Q') = -j\rho\omega \iint_{S_c} G(Q,Q') V_n(Q) dQ \tag{8}$$

Numerical solution of the previous integral equation is based on the discretization of the surface S_c into N elementary areas A_r called patches. The

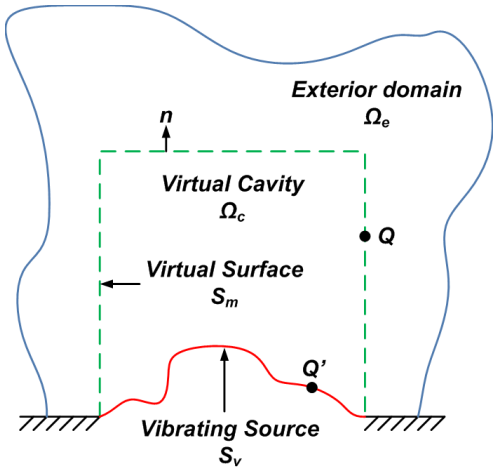

Figure 2: Basic identification problem

discretization of Eq. (8) on patches basis leads to Eq. (9), describing the relation between the space average normal velocity $\bar{v}_r$ on the patch r and the space average pressure $\bar{p}_j$ on the patch j. One can notice that this relation remains true provided that the size of patches is small compared to the wavelength.

$$\bar{p}_j = \sum_{p=1}^{N} Z_{jr} \bar{v}_r \tag{9}$$

In Eq. (9), the space average pressure and velocity are related by the patch impedance Z_{jr}. Consequently, the patch impedance Z_{jr} between the excited patch p and the receiving patch j is defined as the ratio of the space average pressure $\bar{p}_j$ on a patch j and the space average normal velocity $\bar{v}_r$ on a patch p as expressed in Eqs. (10).

$$Z_{jr} = \frac{\bar{p}_j}{\bar{v}_r} \tag{10}$$

Where the space average is defined as $\bar{\bullet}_r = \frac{1}{A_r} \int_{A_r} \bullet \, dA_r$

The basic equation of the iPTF is derived from Eq. (9), where the contribution of patches is separated into patches belonging to the source surface S_v and patches belonging the virtual surface S_m as expressed by Eq. (11).

$$\bar{p}_j = \sum_{k=1}^{P} Z_{jk}\bar{v}_k \; + \; \sum_{i=1}^{M} Z_{ji}\bar{v}_i \tag{11}$$

Where j and i belong to S_m, k belongs to S_v and $N = M + P$

Now, the iPTF formulation can be obtained from Eq. (11) in a straightforward manner. For sake of simplicity, Eq. (11) is written in matrix form (see Eq. (12)) and following notations are considered: $P_j = \bar{p}_j$, $V_i = \bar{v}_i$ and $V_k = \bar{v}_k$

$$\{P_j\} = [Z_{jk}]\{V_k\} + [Z_{ji}]\{V_i\} \tag{12}$$

One has to notice that in matrices $[Z_{ji}]$ and $[Z_{jk}]$, the number of line j represents the number of patch pressure measurements $\{P_j\}$, while the number of column k corresponds to the number of identification patches of source velocity $\{V_k\}$ and i represents the number of patch velocity measurements $\{V_i\}$.

The vector of source velocities $\{V_k\}$ is thus easily obtained after simple matrix manipulation and is the basic equation of the iPTF method.

$$\{V_k\} = [Z_{jk}]^{-1}(\{P_j\} - [Z_{ji}]\{V_i\}) \tag{13}$$

Insofar as the impedances matrices $[Z_{jk}]$ and $[Z_{ji}]$ are numerically computed, only pressures $\{P_j\}$ and velocities $\{V_i\}$ have to be measured on each patch of the virtual surface S_m to calculate the mean patch source velocities $\{V_k\}$. In the iPTF method, the patch pressure $\{P_j\}$ and the patch velocity $\{V_i\}$ are measured with a pressure-velocity (PU) probes. Such PU probes have been assessed by Jacobsen and Jaud [18, 19]. One important point is that velocity field on the virtual surface can be due to direct field from the vibrating surface as well as reflected sound by obstacles placed outside the virtual cavity. Thus, this method is not restricted to anechoic environment and is theoretically independent of sources located outside the measurement area in virtue of the Kirchhoff's integral. Nevertheless, the inversion of the impedances matrices can be difficult, since these matrices are rectangular and ill-conditioned as it will be presented in the section 2.4.

2.3. Computation of patch impedance Z_{jr}

As already said in section 2.2, the patch impedance matrices $[Z_{jk}]$ and $[Z_{ji}]$ are numerically computed. They are derived from the integral formula-

tion (see Eq. (8)) and the expansion on virtual rigid wall cavity modes. To obtain these quantities, we have to calculate the function $G(Q, Q')$ satisfaying Eq. (4). For this purpose, we expand the solution on normal modes of the rigid wall cavity. This leads to the Green's function given by Eq. (14). In appendix A, the detailed calculation of the Green's function is presented.

$$G(Q, Q') = -\sum_n \frac{c^2 \phi_n(Q)\phi_n(Q')}{\Lambda_n(\omega_n^2 - \omega^2 + j\eta_n\omega_n\omega)} \tag{14}$$

Where Λ_n is the norm of the mode n, η_n the modal damping, avoiding singularities when $\omega = \omega_n$.

Then, the pressure $p(Q')$ created by a constant normal velocity $\bar{v}_r$ imposed on a patch r of surface S_r can be calculated from Eq. (15).

$$p\ (Q') = -j\rho\omega c^2 S_r \sum_n \frac{\bar{\phi}_{n_r}\phi_n(Q')}{\Lambda_n(\omega_n^2 - \omega^2 + j\eta_n\omega_n\omega)}\bar{v}_r \tag{15}$$

The patch impedance Z_{jp} between the excited patch p and the receiving patch j is thus given by Eq. (16), where the space average pressure over receiving patches is introduced.

$$Z_{jp} = \frac{\bar{p}_j}{\bar{v}_p} = -\sum_n \frac{j\omega\rho c^2 S_p}{\Lambda_n(\omega_n^2 - \omega^2 + j\eta_n\omega_n\omega)}\bar{\phi}_{n_p}\bar{\phi}_{n_j} \tag{16}$$

Where S_p is the surface of the patch p.

One can also notice that the natural frequencies ω_n and the mode shapes of the virtual rigid wall cavity ϕ_n are obtained by FE calculation, which permits to deal with complex source geometries.

2.4. Some explanations about ill-conditioned impedance matrices

In the iPTF method, impedance matrix $[Z_{jk}]$ has to be inverted. However, in many inverse problems, matrices can be ill-conditioned, which is the case in the present method. Consequently, it is important to identify factors causing the ill-conditioning of $[Z_{jk}]$ matrix. For this purpose, the conditioning number is a good indicator and serves as base for the following discussion. One reminds that $[Z_{jk}]$ matrix relates the number of patches j, where patch pressures $\{P_j\}$ are measured to the number of patches k,where patch source velocities $\{V_k\}$ are identified.

2.4.1. Influence of pressure information on source surface

Let us consider the source surface presented in Fig. (3). To avoid particular cases, this source surface has no symmetries. A virtual cavity is then defined as well as measurement and source patch meshes as shown in Fig. (3). The dimensions of the virtual cavity are about $500 \times 350 \times 400$ mm^3.

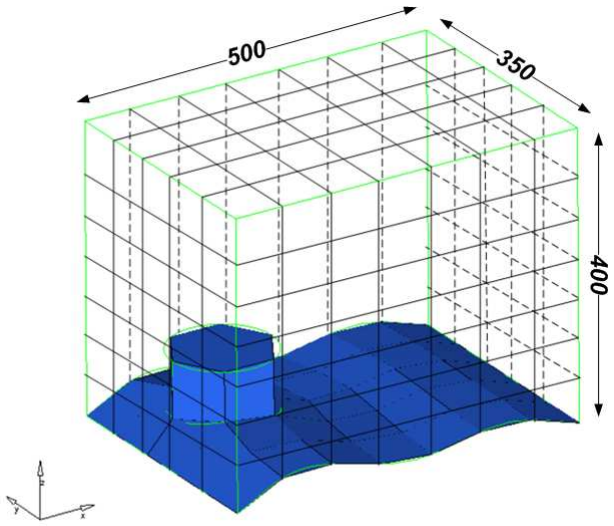

Figure 3: Geometry of the vibrating source and patch mesh definition on surface of the virtual cavity

First of all, we consider the standard way of using the method, where pressure is measured on all virtual surfaces but not on the source surface. In this case, conditioning numbers versus frequency are presented in Fig. (4). The analysis shows that impedance matrix is ill-conditioned. Conditioning number globally decreases with frequency and presents peaks on resonance frequencies of the cavity. To clarify this tendency, we consider a second situation, corresponding to the first one with addition of pressure measurement on the source surface.

The conditioning number, presented in Fig. (4), clearly indicates that impedance matrix is better conditioned. Pressure information on source surface is thus important to decrease the conditioning number. Unfortunately, practically speaking, pressure measurement on source surface is often not possible in real situation. However, it may be sufficient to measure only few

pressure data on the source surface to really decrease the conditioning number. In this way, we assumed that pressure is measured on all the virtual surfaces and on only one patch located in the center of source surface. Result is presented in Fig. (4), with one additional pressure point on the source surface. Above 1200 Hz, the conditioning number is divided by two which represents a real improvement. However, at lower frequency, no significant modifications of the conditioning number appear.

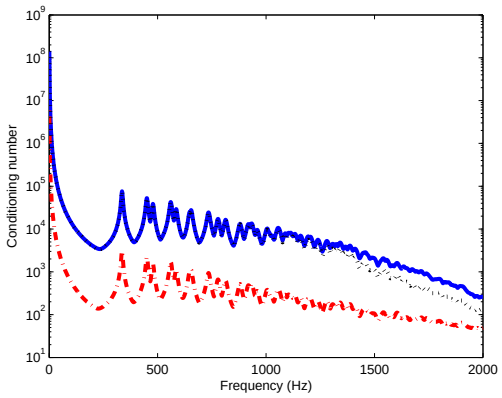

Figure 4: Conditioning number of patch impedance matrices - Comparison between (-) Pressure measured on all the virtual surfaces, (-.-) Pressure measured on all the virtual surfaces and on the source surface and (- -) Pressure measured on all the virtual surfaces and on one patch located in the center of source surface

2.4.2. Influence of the number of pressure control points

From a practical point a view, one can wonder if all the pressure information on virtual surfaces is necessary. For this purpose, we used the same source geometry and virtual cavity as in section 2.4.1, but we only used pressure information measured on the top virtual surface (see Fig. (3)), instead of using pressure information on all the virtual surfaces. Conditioning numbers versus frequency are presented in Fig. (5) for the previous situations. The analysis shows as expected that it is preferable to measure pressure field on all the virtual surfaces to limit the conditioning number.

The conclusion is thus simple, the more measured patch pressure, the lower the conditioning number. Practically, it is recommended to measure

pressure and velocity data on all patches of the virtual surface and if possible on additional points on the source surface. In the rest of this paper, pressure information on source surface is voluntarily not measured insofar as the aim is to find a method to identify properly source velocity without measuring data on the source surface.

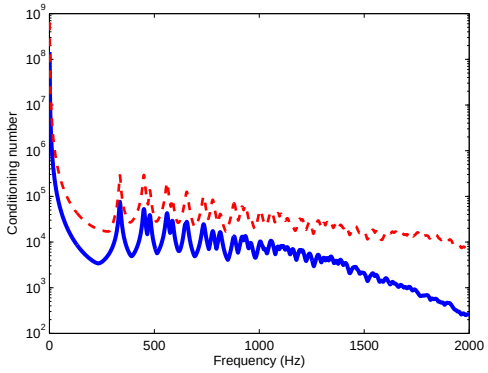

Figure 5: Conditioning number of patch impedance matrices - Comparison between (-) Pressure measured on all the virtual surfaces, (- -) Pressure measured on the top virtual surface

2.4.3. Influence of virtual cavity dimensions

In the iPTF method, the virtual cavity can be arbitrary defined. It is thus interesting to know, if it is preferable to perform measurements on a small or large virtual cavity. To compare results, we consider the same source geometry as in the previous subsection (see Fig. (6)). The virtual cavity smaller than the previous one is almost a parallelepiped with dimensions about $500 \times 350 \times 120$ mm^3 and the patch mesh is defined on virtual surfaces as presented in Fig. (6)). Furthermore, we assumed that pressure and particle velocity are measured on all the virtual surfaces.

Fig. (7) presents conditioning numbers for the large and the small virtual cavities (see Figs. (3) and (6)). This figure shows that patch impedance matrix conditioning number for a small cavity is better at low frequency than that obtained for a large cavity. But when modal overlap is achieved both cavities have similar conditioning numbers. A small cavity is therefore preferable to limit the conditioning number. This point can be associated to

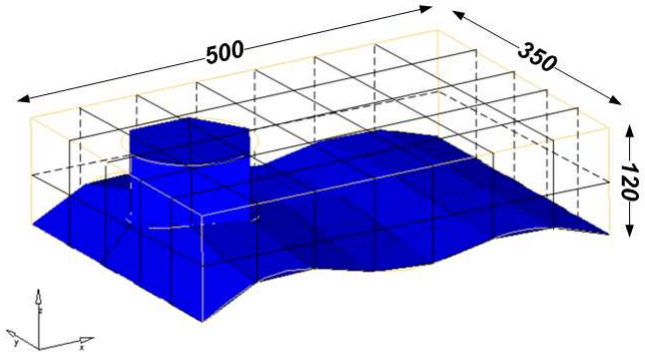

Figure 6: Geometry of the vibrating source and patch mesh definition Geometry of the vibrating source and patch mesh definition on surface of a $500 \times 350 \times 120$ mm^3 virtual cavity

the well-known necessity of holographic methods of making measurements in the nearfield of the source, because of the evanescent nature of acoustic nearfield.

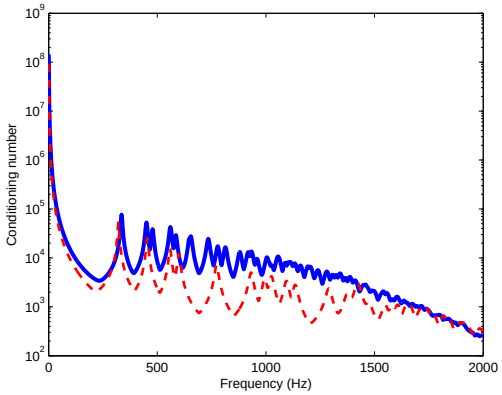

Figure 7: Conditioning number of patch impedance matrices - Comparison between Pressure-Velocity measured on all the virtual surfaces for (-) the large virtual cavity and (- -) the small virtual cavity

2.4.4. Influence of virtual cavity modes

Ill-conditioning can also be due to a bad definition of the virtual volume and patch mesh. Ouisse et al. [16] define a numerical criterion to limit the

ill-conditioning of patch impedance matrices. This criterion stipulates that the order of virtual cavity modes in one direction has to be greater than or equal to the number of patches in the same direction. It corresponds in fact to the number of degrees of freedom necessary to ensure that patches motions are independent. To demonstrate the validity of this criterion, conditioning number is evaluated for a parallelepiped virtual cavity which dimensions are $450 \times 350 \times 130$ mm^3. A patch mesh is then defined on measurement and source surface and natural modes have been extracted up to 2kHz, 3kHz, 4kHz and 5kHz. In each case, patch impedance matrices have been computed in the frequency range of interest [10, 2000 Hz]. As shown in Table 1, the criterion is not respected for modes extrated up to 2 kHz and as a consequence the patch impedance matrix is extremely ill-conditioned (see Fig. (8)). Furthermore, the criterion is respected above 3 kHz and conditioning numbers are very much better than that obtained for modes extracted up to 2 kHz. Nevertheless, a regularization would be compulsory in this configuration but this criterion is required to limit the ill-conditioning of impedance matrices.

Table 1: Comparison between the maximal order of cavity modes and the number of patches along the directions x,y and z

Modal frequency limit	2kHz	3kHz	4kHz	5kHz
Maximal order of modes	$5 \times 4 \times 1$	$7 \times 6 \times 2$	$10 \times 8 \times 3$	$13 \times 10 \times 3$
Number of measurement patches		$6 \times 5 \times 2$		
Number of source patches		6×5		

When virtual cavity has a complex geometry, this criterion is not directly applicable. However, one can say that the number of virtual cavity modes must be at least equal to the number of patches.

3. Numerical and experimental validation of the iPTF method

In this section, we seek to validate the iPTF method numerically and experimentally from a simple set-up. The retained set-up consists of two baffled pistons driven in antiphase as shown in Fig. (9). The chosen test case is voluntarily simple in order to clearly establish how the method is able to localize and separate vibrating sources. The identification area (dimensions:

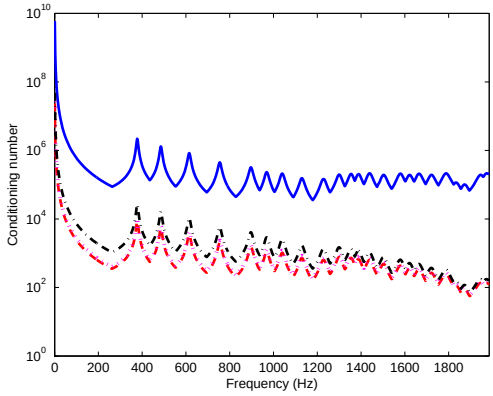

Figure 8: Influence of the maximal cavity modes order on the conditioning number of patch impedance matrices for a $450 \times 350 \times 130$ mm^3 virtual cavity and modes extracted up to (-) 2 kHz, (- -) 3 kHz, (..) 4 kHz and (-.-) 5 kHz

450×350 mm^3) is divided into 30 patches where pressure and particle velocity are assumed constant. Furthermore, the patch impedance matrices computed in this validation section are sufficiently well conditioned to avoid the use of regularization techniques.

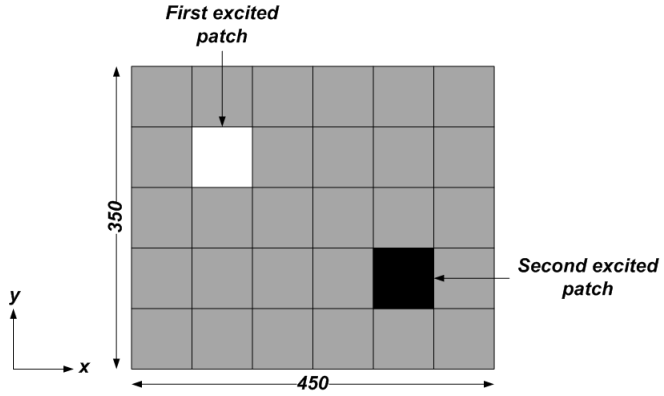

Figure 9: Definition of the validation set-up - Two baffled pistons driven in antiphase

3.1. Numerical validation

3.1.1. Validation of the basic principle

To validate the basic principle given by Eq. (13), we define a parallelepiped virtual cavity measuring $450 \times 350 \times 20$ mm^3 around the source

(see Fig. (10a)). Moreover, in the PTF method, the definition of patch meshes is driven by a wavelength criterion according Ouisse et al. [16]. They have demonstrated that in its direct formulation, the PTF method is applicable with a $\lambda_{ac}/2$ criterion for patch meshes. However, for iPTF method, an additional condition must be considered; the measurement mesh has to be fine enough to obtain a sufficient number of measurement data. In other words, the number of measurement patches has to be larger than the number of identification patches to avoid under-determination of the problem. Based on this observation, the measurement surface is divided into 139 patches and pressure and particle velocity fields are analytically computed at the center of each measurement patch with standard Rayleigh integral method (see appendix B for details).

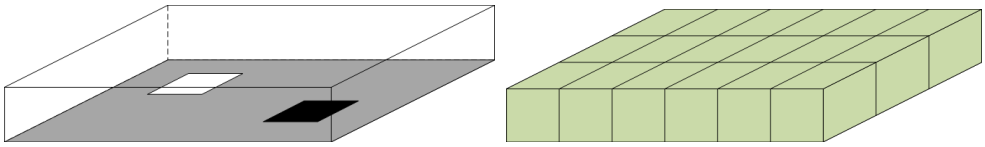

(a) (b)

Figure 10: Definition of (a) the virtual cavity and (b) the patch mesh around the source

The process allows identifying properly the source velocity, since reference and identification maps at 240 Hz slightly differ as shown in Figs. (11) and (12).

3.1.2. Robustness of the iPTF method - Influence of the measurement noise

The measurement noise is an important parameter in the results accuracy. In order to analyse the influence of measurement uncertainties, we propose to slightly modify the exact pressure and particle velocity fields analytically computed by introducing two independent Gaussian random variables ΔQ and $\Delta\phi$, simulating errors on the magnitude and the phase of measurement data [20]:

$$\begin{cases} \widetilde{P} = P^{exact}.\Delta Q_p.e^{j\Delta\phi} \\ \widetilde{V} = V^{exact}.\Delta Q_v.e^{j\Delta\phi} \end{cases} \tag{17}$$

Where $\Delta Q_p = p|P^{exact}|X + 1$ and $\Delta\phi = \arctan(p)Y$, with p the noise percentage and (X,Y) two independent Gaussian random variables.

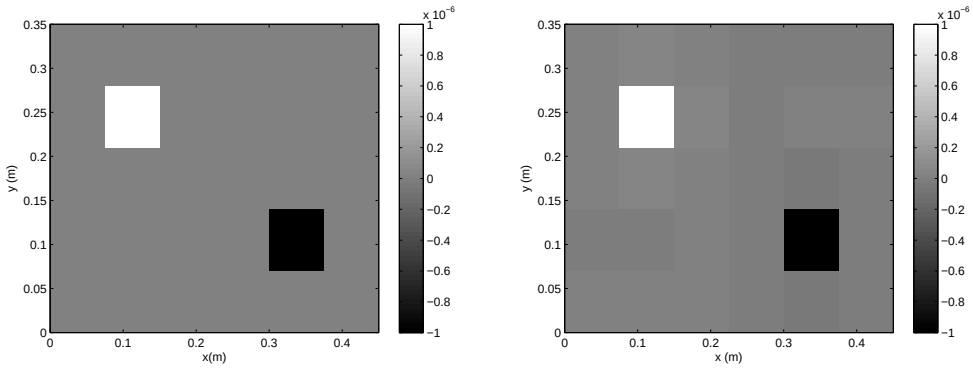

(a) (b)

Figure 11: Numerical validation for a $450 \times 350 \times 20$ mm^3 virtual cavity - Comparison of (a) the reference map and (b) the identified map obtained with the iPTF method at 240 Hz

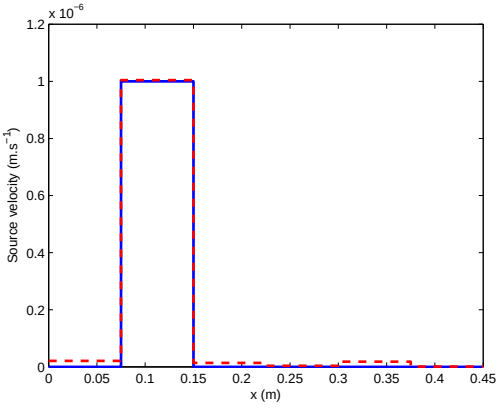

Figure 12: Numerical validation for a $450 \times 350 \times 20$ mm^3 virtual cavity - Comparison of source velocity along a line (x,0.245 m) across the prediction plane at 240 Hz, (-) Reference, (- -) Identification

Figs. (13) and (14) present the influence of measurement uncertainties on identifications for $p = 30\%$. We can thus notice that the measurement noise has a limited influence on the identification accuracy, insofar as the magnitude and spatial distribution of source velocities are only marginally affected. Consequently, the proposed method appears to be robust with

respect to measurements uncertainties.

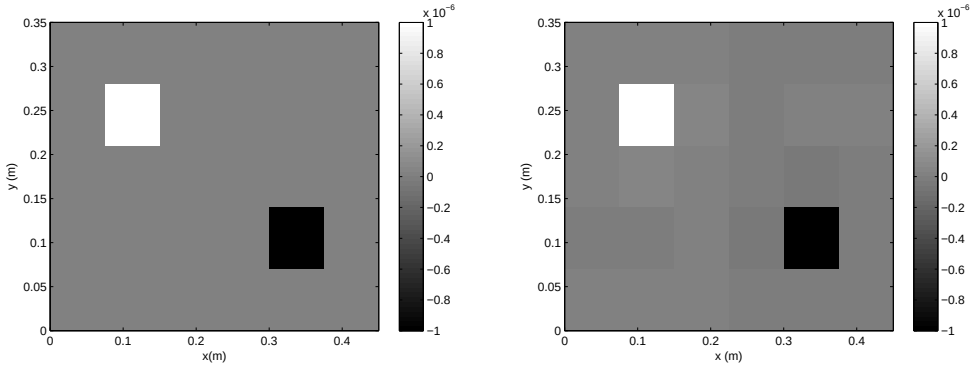

(a) (b)

Figure 13: Numerical validation for a $450 \times 350 \times 20$ mm^3 virtual cavity - Comparison between (a) the reference map and the identified maps obtained for (b) (b)$p = 30\%$ at 240 Hz

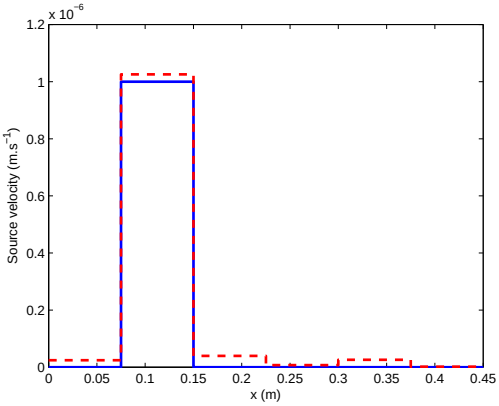

Figure 14: Numerical validation for a $450 \times 350 \times 20$ mm^3 virtual cavity - Comparison of source velocity along a line (x,0.245 m) across the prediction plane at 240 Hz, (-) Reference, (- -) Identification for $p = 30\%$

3.2. Robustness of the iPTF method - Influence of correlated disturbing source

When measurements are performed *in situ*, correlated sources can modify the pressure and the particle velocity fields measured around the source to

identify. Consequently, virtual sources are likely to appear on the hologram due to the bad estimation of acoustic field in the measurement area. As underlined in section 2, the iPTF method is theoretically independent of the presence of external sources. To prove this theoretical fact, a third piston is inserted in the rigid baffle, whereof velocity is 5 times bigger than that of the first piston (see Fig. (15)). This third disturbing piston modifies the acoustic field computed at the center of the measurement patches. As an exemple, the mean square pressure is increased by 6.5 dB at 240 Hz, while the mean square particle velocity is increased by 3.5 bB at the same frequency.

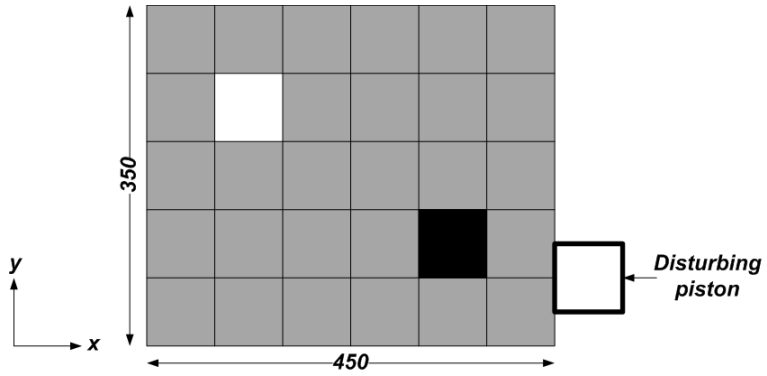

Figure 15: Location of the disturbing piston outside the identification area

Fig. (16) presents the comparison of the spatial distribution of reference source velocity with the identified one obtained in presence of a disturbing acoustic source. Maps prove that the source velocity can be properly identified in presence of a disturbing source.

3.2.1. Influence of the virtual cavity dimensions

The dimensions of the virtual cavity is essential in the identification process since the more we measure far from the source, the more we lose the near field information related to the evanescent waves. In that case, it is hard to identify precisely the source velocity because of the lack of information. To demonstrate the influence of the cavity dimensions on the identification, we define a virtual cavity which dimensions are $450 \times 350 \times 130$ mm^3. Furthermore, the measurement surface is divided into 259 patches. As shown in Fig. (18), the iPTF method succeeds in identifying source velocities. However, as classically observed in other holographic methods (NAH or iBEM), the

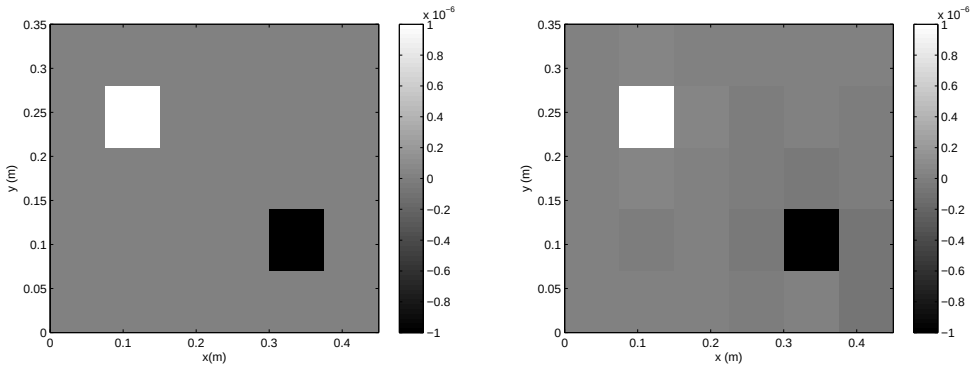

(a) (b)

Figure 16: Numerical validation for a $450 \times 350 \times 20$ mm^3 virtual cavity in presence of an external disturbing source - Comparison of (a) the reference map and (b) the identified map obtained at 240 Hz

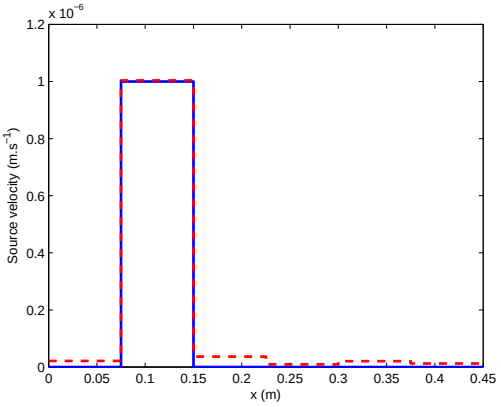

Figure 17: Numerical validation for a $450 \times 350 \times 20$ mm^3 virtual cavity in presence of an external disturbing source - Comparison of source velocity along a line (x,0.245 m) across the prediction plane at 240 Hz, (-) Reference, (- -) Identification

source localization and separation are less clear because of the absence of near field information in the considered data.

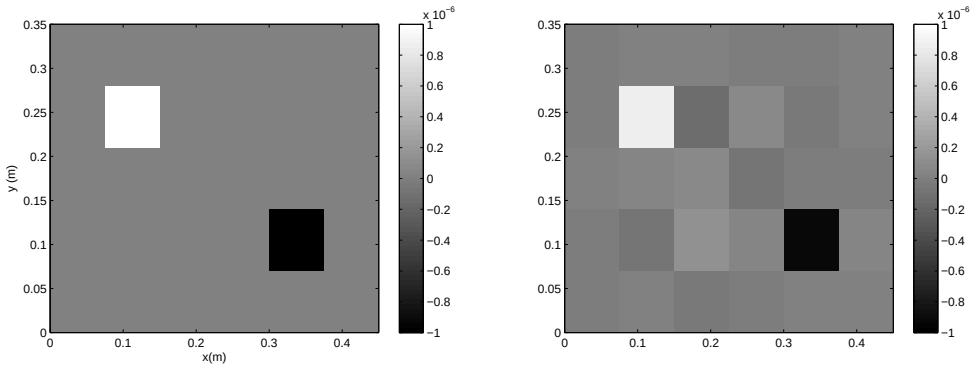

Figure 18: Numerical validation for a $450 \times 350 \times 130$ mm^3 virtual cavity - Comparison between (a) the reference map and (b) the identified map obtained with the iPTF method at 240 Hz

3.3. Experimental validation

3.3.1. Experimental set-up

The experimental validation consists in reproducing as reliably as possible the set-up used for the numerical validation, in order to evaluate the applicability and the robustness of the method in a non anechoic environment. For this purpose, the acoustic baffle consists of a wooden thick plate of $700 \times 600 \times 40$ mm^3, in which two loudspeakers fed by a white noise are inserted. Furthermore, the identification area is materialized on the rigid baffle as shown in Fig. (19).We can also notice that measurements were performed in a non anechoic chamber and consequently reflected sound from room boundaries was present. Finally, reference and acoustic field measurements were carried out with a PU probe in the very nearfield of the source (5 mm from the acoustic source) and a microphone was used as phase reference.

Like in previous sections, we define around the identification area the same patch meshes as those used in the numerical validation. It is relevant to remind that space averaged data of pressure and particle velocity on patches are represented by one measurement point at the center of the patch. By this way, a positioning error of the PU probe can influence the quality of the experimental results. Of course, other factors can come into account like normal vectors orientation for particle velocity measurements or uncertainties due to transducers quality.

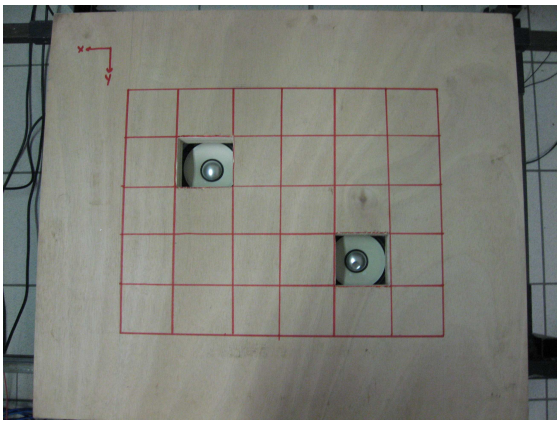

Figure 19: Experimental set-up

In the following, we use an indicator ϵ which allows thoroughly derter-mining the identification error of the iPTF method. This indicator is define as in Eq. (18).

$$\epsilon = 10\log\left|\frac{V_{id}^2}{V_{ref}^2}\right| \tag{18}$$

Where V_{ref} is the source velocity measured in the very nearfield of the source and V_{id} is the identified source velocity.

3.3.2. Validation of the basic principle

The experimental validation of the basic principle is performed by reproducing the numerical experiment used in section 3.1. When applying the iPTF method from experimental data, a good agreement between measured and identified source velocity is observed both in magnitude and spatial distribution (see Figs. (20) and (21)). The analysis of Fig.(20) shows actually that the identification error on the first excited patch ((x, y) =(0.1125 m,0.245 m)) does not exceed 1 dB on all the frequency range.

3.3.3. Robustness of the iPTF method - Influence of correlated disturbing source

To test the robustness of the method in presence of a correlated disturbing source, we used the same virtual cavity as in the previous case and a third loudspeaker located outside the measurement area was added (see Fig.

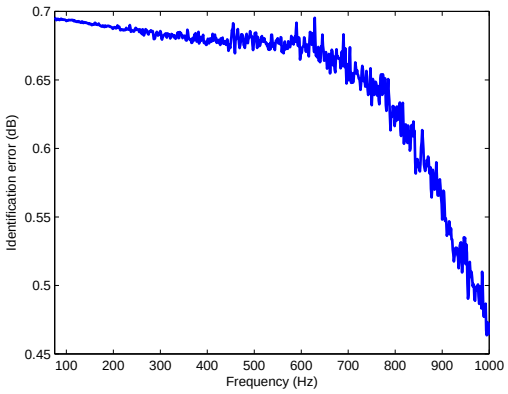

Figure 20: Experimental validation for a $450 \times 350 \times 20$ mm^3 virtual cavity - Identification error on the first excited patch (x, y) =(0.1125 m,0.245 m)

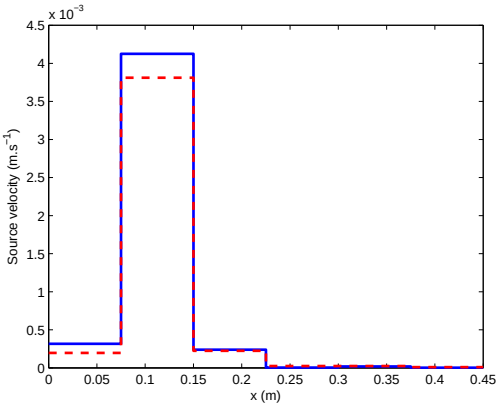

Figure 21: Experimental validation for a $450 \times 350 \times 20$ mm^3 virtual cavity - Comparison of source velocity along a line (x,0.245 m) across the prediction plane at 240 Hz, (-) Reference, (- -) Identification

(22)). A reference measurement was performed again to take into account the acoustic field modifications due to the disturbing source.
The pressure power spectrum measured on a patch of the measurement surface with and without disturbing source highlights the influence of the disturbing source. Disturbing pressure was in general of the same order as the primary source pressure and at certain frequencies differed from more than

5 dB (see Fig. (23)).

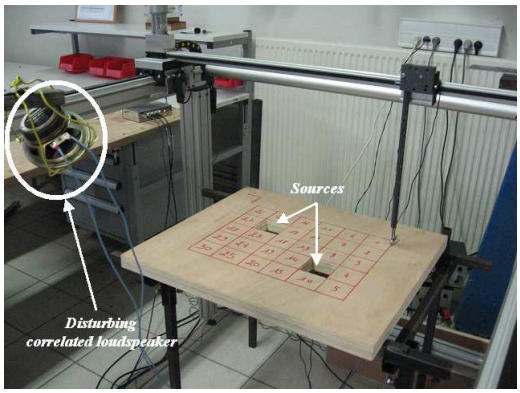

Figure 22: Experimental set-up - Location of the disturbing source

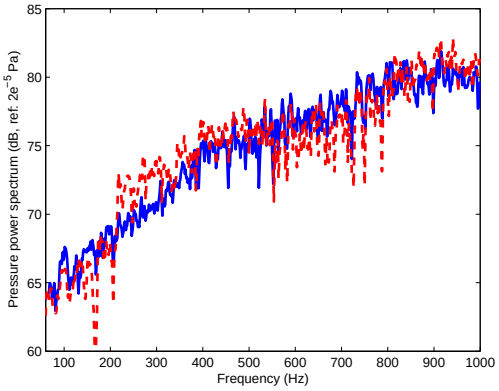

Figure 23: Comparison between the pressure power spectrum obtained on a patch of the measurement surface (-) without and (- -) with the disturbing source versus frequency

The iPTF method allows determining a source velocity, which magnitude differs from reference by less than 1 dB on all the frequency range, as shown in Fig. (24) presenting the identification error on the first excited patch ((x, y) =(0.1125 m,0.245 m)). Moreover, the Fig. (25) presents a comparison between the reference map and the identified one. This comparison confirms the ability of the method to reconstruct the spatial source velocity distribution in presence of an external stationary disturbing source.

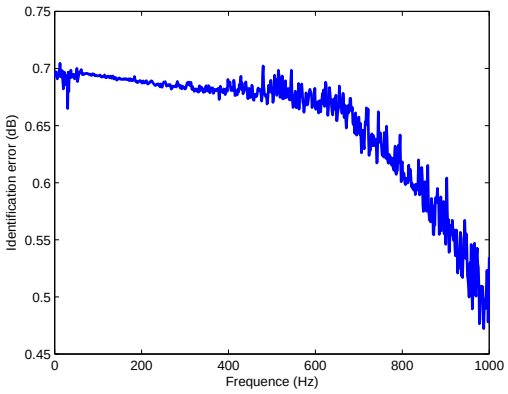

Figure 24: Experimental validation for a $450 \times 350 \times 20$ mm^3 virtual cavity in presence of an external correlated disturbing source - Identification error on the first excited patch (x, y) =(0.1125 m,0.245 m)

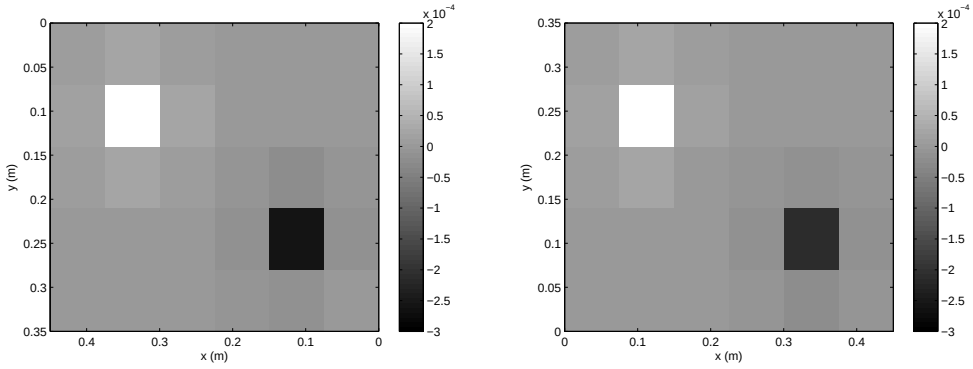

(a) (b)

Figure 25: Experimental validation for a $450 \times 350 \times 20$ mm^3 virtual cavity in presence of an external correlated disturbing source - Comparison between (a) the reference map and (b) the identification map obtained experimentally in presence of a disturbing source with the iPTF method at 240 Hz

3.3.4. Influence of the virtual cavity dimensions

As already evoked in the numerical validation of the method, the more we measure the sound field far from the source, the more we lose information related the evanescent waves. The aim of this section is to know how experi-

mentally the absence of near field information affects the identification accuracy. For this purpose, we use the virtual cavity of dimensions $450\times350\times130$ mm^3 defined in section 3.2.1. In this case too, the iPTF method gives quite satisfaying results in both magnitude and spatial distribution (see Figs. (26) and (27)). However, Fig. (26) shows that the identification is less accurate in magnitude than that performed on a cavity of reduced dimensions. The discrepancy is however acceptable up to 425 Hz, where the height of the virtual cavity reaches $\frac{\lambda}{6}$ ($\frac{340}{6\times425} \approx 0.13\ m$). Nevertheless, the method succeed in localizing the two louspeakers below 425 Hz.

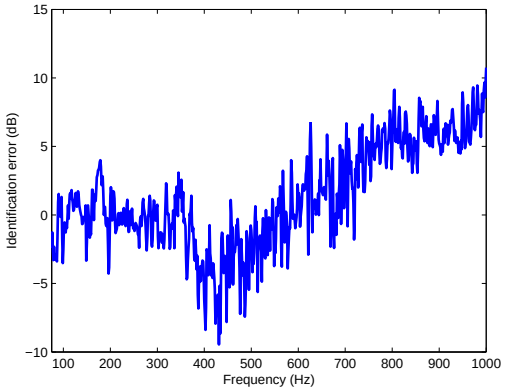

Figure 26: Experimental validation for a $450\times350\times130$ mm^3 virtual cavity - Identification error on the first excited patch (x, y) =(0.1125 m,0.245 m)

4. Conclusion

The iPTF method allows identifying source velocities on complex structures. In this paper, the theoretical background as well as the measurement methodology have been introduced. In the method, both pressure and particle velocity fields have to be measured on the virtual cavity surfaces. This is quite simple when using PU probes. To prove the ability of the method, an experimental validation has been set up on two baffled pistons driven in antiphase.
As classically observed in holographic methods, one of the main drawbacks remains the loss of the near field information when measuring acoustic field far from the source.

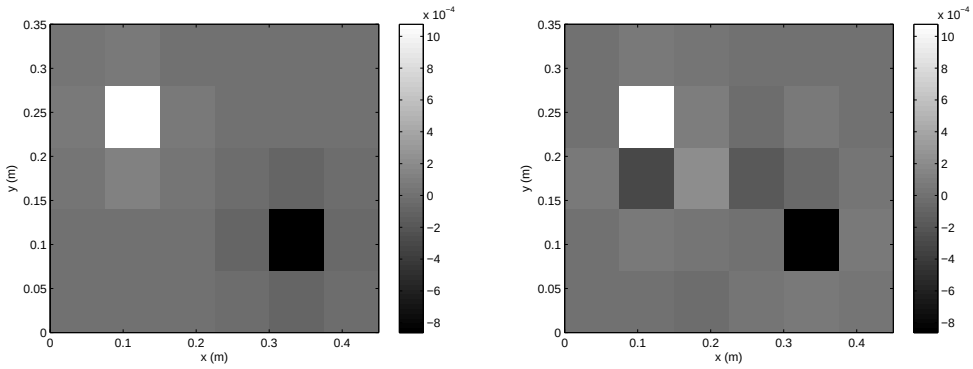

Figure 27: Experimental validation for a $450 \times 350 \times 130$ mm^3 virtual cavity - Comparison between (a) the reference map and (b) the identified map obtained experimentally with the iPTF method at 240 Hz

However, the combined use of integral formulation, FEM as a solver and the double measurement of pressure and particle velocity fields allows overcoming some limitations of classical methods associated to simple structure geometry. Thus, the independence of the method with respect to external stationnary sources and its applicability to complex shape structures are the main advantages of the iPTF method. Finally, further applications of the method on more complex structures than that presented in this article, namely an L-shape plate and a vehicle precatalyst, can be found in Refs. [21] and [22]

References

[1] E.G. Williams, J.D. Maynard, and E. Skudrzyk. Sound source reconstructions using a microphone array. *Journal of the Acoustical Society of America*, 68:340–344, 1980.

[2] E.G. Williams. The nearfield acoustical holography (NAH) experimental method applied to vibration and radiation in light and heavy fluids. *Computers & Structures*, 65 (3):323–335, 1997.

[3] E.G. Williams. *Fourier Acoustics: Sound Radiation and Nearfield Acoustical Holography*, chapter 3 - The Inverse Problem: Planar

Nearfield Acoustical Holography, pages Pages 89–114. Academic Press, 1999.

[4] E.G. Williams. *Fourier Acoustics: Sound Radiation and Nearfield Acoustical Holography*, chapter 5 - The Inverse Problem: Cylindrical NAH, pages 149–182. Academic Press, 1999.

[5] E.G. Williams. *Fourier Acoustics: Sound Radiation and Nearfield Acoustical Holography*, chapter 7 - Spherical Nearfield Acoustical Holography, pages 235–249. Academic Press, 1999.

[6] B. K. Bai and J. G. Ih. On the reconstruction of the vibro-acoustic field over the surface enclosing space using the boundary element method. *Journal of Acoustical Society of America*, 100:3003–3016, 1996.

[7] F. Martinus. An advanced noise source identification technique using the inverse boundary-element method. *Journal of Acoustical Society of America*, 118 (3):1916, 2005.

[8] S. F. Wu. Hybrid nearfield acoustical holography. *Journal of Acoustical Society of America*, 115:207–217, 2004.

[9] X. Zhao and S.F. Wu. Reconstruction of vibro-acoustic fields using hybrid nearfield acoustic holography. *Journal of Sound and Vibration*, 282 (3):1183–1199, 2004.

[10] S. F. Wu and J. Yu. Reconstructing interior acoustic pressure field via helmholtz equation least-squares method. *Journal of Acoustical Society of America*, 104:2054–2060, 1998.

[11] N. E. Rayess and S. F. Wu. Experimental validations of the hels method for reconstructing acoustic radiation from a complex vibrating structure. *Journal of Acoustical Society of America*, 107:2955–2964, 2000.

[12] S.F. Wu and X. Zhao. Combined helmholtz equation least-squares method for reconstructing acoustic radiation from arbitrarily shaped objects. *Journal of Acoustical Society of America*, 112:179–188, 2002.

[13] Q. Leclère and B. Laulagnet. An alternative acoustic imaging technique to improve capabilities of microphone array measurements. In *Proceedings of November 2005, St Raphael, France*, 2005.

[14] Q. Leclère, B. Laulagnet, and L. Polac. Application of an innovative acoustic imaging technique to assess acoustic power maps of a gasoline engine. In *Proceedings of Forum Acusticum 2005, Budapest, Hungary*, 2005.

[15] L. Maxit, C. Cacciolati, and J.L. Guyader. Airbone noise prediction using patch acoustic impedance. In *Proceedings of ICSV9, Orlando, United-States*, 2002.

[16] M. Ouisse, L. Maxit, C. Cacciolati, and J.L. Guyader. Patch transfer functions as a tool to couple linear acoustic problems. *Journal Vibration Acoutics, Transactions of the ASME*, 127:458–466, 2005.

[17] N. Totaro, B. Andro, C. Peteul, and J.L Guyader. Extension of the Patch Tranfer Functions method (PTF Method) to high frequency domain (sub-cavities decomposition). In *Proceedings of Inter-Noise, Istanbul, Turkey*, 2007.

[18] F. Jacobsen and V. Jaud. A note on the calibration of pressure-velocity sound intensity probes. *Journal of Acoustical Society of America*, 120 (2):830–837, 2006.

[19] F. Jacobsen and V. Jaud. Statistically optimized near field acoustic holography using an array of pressure-velocity probes. *Journal of Acoustical Society of America*, 121 (3):1550–1558, 2007.

[20] C. Pezerat and J.L. Guyader. Two inverse methods for localization of external sources exciting a beam. *Acta Acustica*, 3:1–10, 1995.

[21] M. Aucejo, N. Totaro, and J-L. Guyader. Identification of source velocities with iPTF (inverse Patch Transfer Functions method). In *Proceedings of Acoustics08, Paris, France*, 2008.

[22] N. Totaro, C. Sandier, and Guyader J-L. Identify velocity of a complex source with iPTF method. In *Proceedings of ICSV15, Daejon, South Korea*, 2008.

A. Calculation of Green's function by modal approach

The Green's identity defined in Eq. (2) is then used, where Φ is the mode shape ϕ_n of the virtual rigid wall cavity Ω_c satisfying Eq. (19) and Ψ is the function G satisfying Eq. (20).

$$\begin{cases} \Delta\phi_n(Q) + k_n^2\phi_n(Q) = 0 & \forall n, \forall Q \in \Omega_c \\ -\dfrac{1}{j\rho\omega}\dfrac{\partial\phi_n}{\partial n}(Q) = 0 & \forall\ n, \forall\ Q \in S_c \end{cases} \tag{19}$$

$$\begin{cases} \Delta G(Q,Q') + k^2 G(Q,Q') = 0 & \forall\ (Q,Q') \in \Omega_c \\ \dfrac{\partial G}{\partial n}\ (Q,Q') = \delta(Q-Q') & \forall\ (Q,Q') \in A_p \\ \dfrac{\partial G}{\partial n}\ (Q,Q') = 0 & \forall\ (Q,Q') \in S_c \setminus A_p \end{cases} \tag{20}$$

Consequently, using Eqs. (2), where $\Phi = \phi_n$ and $\Psi = G$, (20) and (19), we obtain the integral equation given by Eq. (21).

$$\phi_n(Q') = \iiint_{\Omega_c} (k^2 - k_n^2)\phi_n(Q)G(Q,Q')dQ \tag{21}$$

The function G is now determined by expansion on the modal basis $\phi_n(Q)$:

$$G(Q,Q') = \sum_n g_n(Q')\phi_n(Q) \tag{22}$$

Using this decomposition in Eq. (21), one obtains:

$$g_n(Q') = -\frac{c^2\phi_n(Q')}{\Lambda_n(\omega_n^2 - \omega^2)} \tag{23}$$

Where the norm of modes is such as $\iiint_{\Omega_c} \phi_n(Q)\phi_q(Q)d\Omega_c = \Lambda_n\delta_{nq}$. One obtains therefore the following expression:

$$G(Q,Q') = -\sum_n \frac{c^2\phi_n(Q)\phi_n(Q')}{\Lambda_n(\omega_n^2 - \omega^2)} \tag{24}$$

The patch impedance between a source patch k and a reception patch j is then:

$$Z_{jk} = -\sum_n \frac{j\omega\rho c^2 S_k}{\Lambda_n(\omega_n^2 - \omega^2)}\bar{\phi_{n_k}}\bar{\phi_{n_j}} \tag{25}$$

Obviously in the Eqs.(24) and (25), this modal composition presented problems at resonant frequencies. To avoid these difficulties, one introduces the modal damping of fluid η_n, which is a constant in this study. Therefore, one replaces in the denominator the term $\omega_n^2 - \omega^2$ by the term $\omega_n^2 - \omega^2 + j\eta_n\omega_n\omega$.

B. Radiation of a baffled piston

The Rayleigh integral formulation of a baffled piston is used to compute its radiation as expressed in Eq. (26).

$$\begin{cases} p(M) = j\rho\omega \displaystyle\int_S V(Q)G(M,Q)dQ \\ G(M,Q) = \dfrac{e^{-jkR}}{2\pi R} \end{cases} \tag{26}$$

$$V(Q) = \begin{cases} \bar{V}_n & \forall\ Q \in S_{piston} \\ 0 & \text{elsewhere} \end{cases} \tag{27}$$

However, insofar as the dimension of the piston is not negligible, the integral over the piston area is discretized into $n_x \times n_y$ points. Consequently, Eqs. (26) and (27) become:

$$\begin{cases} p(M_r) = j\rho\omega\bar{V}_n \displaystyle\sum_k \frac{e^{-jkR_{kM_r}}}{2\pi R_{kM_r}} \Delta x_k \Delta y_k \\ R_{kM_r} = \sqrt{(x_{M_r} - x_k)^2 + (y_{M_r} - y_k)^2 + (z_{M_r} - z_k)^2} \end{cases} \tag{28}$$

Where $(x_{M_r}, y_{M_r}, z_{M_r})$ are the coordinates of the center of the patch r and (x_k, y_k, z_k) are the coordinates of the point k belonging to the piston.

The particle velocity is then easily obtained at the center of the patch r by using the Euler's equation defined in Eq. (29):

$$V(M_r) = -\frac{1}{j\rho\omega}\bar{V}_n \frac{\partial p}{\partial n_e}(M_r) \tag{29}$$

Where n_e is the external normal vector to the virtual cavity.